

# Machine learning prediction of plasma behavior from discharge configurations on WEST

Chenguang Wan<sup>1,3</sup>, Feda Almuhsen<sup>2,\*</sup>, Philippe Moreau<sup>2</sup>, Rémy Nouailletas<sup>2</sup>, Zhisong Qu<sup>1,\*</sup>, Youngwoo Cho<sup>1</sup>, Robin Varennes<sup>1</sup>, Kyungtak Lim<sup>1</sup>, Kungpeng Li<sup>1</sup>, Jia Huang<sup>3</sup>, Weidong Chen<sup>4</sup>, Jiangang Li<sup>3</sup>, and Xavier Garbet<sup>1,2</sup>

1. School of Physical and Mathematical Sciences, Nanyang Technological University, Singapore 637371, Singapore

2. CEA, IRFM, F-13108 Saint Paul-lez-Durance, France

3. Institute of Plasma Physics, Hefei Institutes of Physical Science, Chinese Academy of Sciences, Hefei 230031, China

4. School of Information Science and Technology, University of Science and Technology of China, Hefei 230093, China

E-mail: [feda.almuhsen@cea.fr](mailto:feda.almuhsen@cea.fr) and [zhisong.qu@ntu.edu.sg](mailto:zhisong.qu@ntu.edu.sg)

**Abstract.** Accurately predicting plasma behavior based on discharge configurations is essential for the safe and efficient operation of tokamak experiments. While physics-based integrated modeling codes provide valuable insights, their high computational cost limits their applicability for fast scenario design and control optimization. In this study, we propose a transformer-based machine learning model to predict key global plasma parameters on the WEST tokamak, including the normalized beta ( $\beta_n$ ), toroidal beta ( $\beta_t$ ), poloidal beta ( $\beta_p$ ), plasma stored energy ( $W_{\text{mhd}}$ ), safety factor at the magnetic axis ( $q_0$ ), and safety factor at the 95% flux surface ( $q_{95}$ ). The model uses only signals that can be defined before the discharge, such as magnetic coil currents, auxiliary heating power, plasma current reference, and line-averaged plasma density. Trained on 550 discharges from the WEST campaigns, the model demonstrates an average mean square error (MSE) loss of 0.026, an average coefficient of determination  $R^2$  of 0.94, and achieves inference times on the order of 0.1 seconds. These results highlight the potential of data-driven surrogate models for assisting in discharge planning, scenario evaluation, and real-time control of tokamak plasmas.

*Keywords:* discharge prediction, WEST, machine learning, transformer

## 1. Introduction

Any plasma discharge needs to be prepared in advance using a discharge schedule editor, in which all tokamak settings are defined. In order to optimize the tokamak operation, these settings must be assessed using a tokamak simulator in order to check the feasibility of the preset discharge scenario.

Predicting plasma behavior from the inputs taken from the discharge schedule editor in tokamaks has traditionally relied on first-principles physics codes, commonly referred to as "Integrated Modeling". These include ETS [1], PTRANSP [2], TSC [3], NICE [4], CRONOS [5], JINTRAC [6], METIS [7], ASTRA [8], RAPTOR [9], and TOPICS [10], etc. While these codes simulate key physical processes with high fidelity, their substantial computational cost makes them unsuitable for fast or real-time prediction tasks.

This is especially true when we need to quickly predict zero-dimensional parameters, such as plasma stored energy  $W_{mhd}$ , toroidal beta  $\beta_n$ , safety factor  $q$  at the magnetic axis  $q_0$ , from a given set of coil currents and preset parameters. Moreover, in practical applications, integrated models involve approximations, model coupling assumptions, and parameter uncertainties that constrain their achievable accuracy. Some real-time-oriented frameworks, such as RAPTOR [9, 11], partially address computational efficiency, but rely heavily on reduced physics models. Their predictive accuracy depends on empirical coefficients, including transport scalings and source models, as well as careful tuning, scenario-specific calibration, and expert knowledge of the device and discharge conditions. While such approaches offer strong physics consistency, control robustness, and interpretability, they often sacrifice shot-by-shot fidelity and have limited ability to capture hidden correlations present in large experimental datasets.

Data-driven methods offer a way to bridge this gap by learning the input-output mapping directly from experimental data, thereby bypassing the need to solve first-principles equations repeatedly. Because of this advantage, researchers in the fusion community have widely adopted data-driven approaches to study a range of problems. Early applications focused on disruption prediction [12–15]. More recent studies have further advanced this area: the first domain-adaptation framework for cross-tokamak disruption prediction achieved clear gains [16], and physics-guided feature extraction has shown clear benefits when data are limited while also improving model interpretability [17]. Additional applications include magnetic field control [18], a surrogate model for the Ion Temperature Gradient (ITG) mode [19], surrogate model of QualiKiz [20], tearing mode control [21], the first real-time avoidance of density-limit disruptions in J-TEXT [15], the last-closed flux surface reconstruction [22, 23], electron temperature profile reconstructions [24], equilibrium reconstruction [25, 26], equilibrium solver [27], missing electron temperature reconstruction [28], density profile inversion [29], radiation power estimation [30], confinement time prediction with uncertainty quantification [31], instability identification [32], neutral beam effect estimation [33], confinement state classification [34], scaling law determination [35, 36], density limit analysis [37], plasma detachment prediction [38], imaging neutral particle analyzer [39], the direct control of tokamak parameters [18, 21], and plasma magnetic measurement estimation [40].

Furthermore, some data-driven approaches have explored full discharge prediction [41–43]. These models do not rely solely on configurations but also incorporate signals such as gas puffing system data, which are hard to determine prior to a discharge and are influenced by the evolving plasma state during the discharge. This dependence constrains their generalizability and practical applicability.

In this study, we developed a transformer-based machine learning model that utilizes only signals that can be directly controlled or feedback-regulated. Compared to previous works [41,

42], our model does not rely on the state of any specific discharge process, thereby enhancing its practical applicability. Specifically, we successfully reproduced six key zero-dimensional global parameters on the Tungsten (W) Environment in Steady-State Tokamak (WEST) by inputting 19 signals, including poloidal field coil currents, auxiliary heating, plasma reference current, and plasma electron density measurements at the magnetic axis.

Our model achieves an average MSE of 0.026, an average coefficient of determination  $R^2$  of 0.94, and an inference time of  $\sim 0.1$  seconds, enabling large-scale control parameter sweeps and optimization tasks. The dataset comprises 550 stable and reproducible discharges from WEST campaigns, all conducted under well-controlled conditions with good wall conditions. This consistency ensures the robustness and applicability of the model in similarly controlled experimental settings.

The remainder of this paper is organized as follows. Section 2 describes the dataset preparation and the analysis of the input and output signals. Section 3 outlines the machine learning methodology. Section 4 presents the model results along with the corresponding analysis. Finally, Section 5 presents a brief conclusion and future directions.

## 2. Dataset

The WEST tokamak is equipped with a comprehensive suite of diagnostic systems, including magnetic diagnostics [44] and plasma state diagnostics [45–47], among others. In the present study, as shown in table 1, the input signals include the power and corresponding phase of the Lower Hybrid Wave (LHW) Current Drive and Heating System, the power of the Ion Cyclotron Resonance Heating (ICRH) System, the reference plasma current, the currents in the Poloidal Field (PF) coils, and the real-time measured plasma line-average density. The output signals include normalized beta  $\beta_n$ , toroidal beta  $\beta_t$ , poloidal beta  $\beta_p$ , plasma stored energy  $W_{mhd}$ , safety factor  $q$  at magnetic axis  $q_0$  and safety factor  $q$  at the 95% flux surface.

It should be noted that we use  $n_{e\_real}$  as a proxy that captures the combined influence of the fueling strategy and wall conditions. In WEST, the electron density is primarily controlled through the fueling system [48], e.g. the gas injection system. However, this control is neither instantaneous nor one-to-one. The fueling system exhibits a relatively long response time, and the achieved density depends nonlinearly on wall conditions and turbulent transport. The main objective of the present work is to predict plasma responses from discharge design parameters, also referred to as experimental proposals, in which the target density is assumed to be achievable in the experiment through feedback control.

A total of 550 discharges, ranging from discharge #57381 to #60286, were initially selected from the WEST database. Discharges with durations less than 2 seconds were excluded, as the ramp-up phase in the WEST tokamak typically takes about 2 seconds. Such short discharges are usually indicative of abnormal events and were not included in the analysis. All selected signals were uniformly resampled at 1 kHz from the start of each discharge and aligned to a common time base. The data were saved in HDF5 format on a discharge-by-discharge basis, resulting in approximately 15 gigabytes of original data. Across the full dataset, the total Lower Hybrid Wave (LHW) power ranges from 0 to  $\sim 4$  MW, while the total Ion Cyclotron Resonance Heating (ICRH) power ranges from 0 to  $\sim 3.1$  MW. The plasma current  $I_p$  spans from  $\sim 100$  to  $\sim 700$  kA, with most discharges concentrated around 400, 500, and 700 kA. The electron density varies from  $\sim 1.0 \times 10^{19}$  to  $\sim 6.2 \times 10^{19} \text{ m}^{-3}$ . The normalized beta  $\beta_n$  ranges from 0.17 to 1.01, the poloidal beta  $\beta_p$  from 0.33 to 1.57, and the toroidal beta  $\beta_t$  from 0 to  $3 \times 10^{-3}$ . The plasma stored energy  $W_{mhd}$  ranges

**Table 1:** The list of signals. A signal name ending with "\_real" indicates the real diagnostic data during the tokamak discharge process. The signal name ending with "\_ref" indicates that the data is reference data, i.e. nominal signals in the Discharge Control System (DCS) of WEST.

Signals	Physics meanings	# of channels	sampling rate
Output signals		6	
$\beta_n$	Normalized beta	1	1 - 12 Hz
$\beta_t$	Toroidal beta	1	1 - 12 Hz
$\beta_p$	Poloidal beta	1	1 - 12 Hz
$W_{mhd}$	Plasma stored energy	1	1 - 12 Hz
$q_{95}$	Safety factor q at the 95% flux surface	1	1 - 12 Hz
$q_0$	Safety factor q at the magnetic axis	1	1 - 12 Hz
Input signals		19	
LHW_real	Power of Lower Hybrid Wave (LHW) Current Drive and Heating System	4	1 kHz
ICRH_real	Power of Ion Cyclotron Resonance Heating (ICRH) System	3	1 kHz
$I_p$ _ref	Reference of plasma current	1	1 kHz
$n_e$ _real	Actual line-average electron density at the magnetic axis	1	1 kHz
PF_real	Current of Poloidal Field (PF) coils	10	1 kHz

from 212 to 342 kJ. The safety factor  $q_{95}$  spans from 0.88 to 8.64, while the central safety factor  $q_0$  ranges from 0.96 to 3.25. The details of the distribution are given in Appendix A figure 5.

The selection of input signals was guided by the experience of operators and plasma physicists. To further validate the relevance of these inputs prior to training the machine learning model, and to assess the relationships between input and output signals, we computed both the Granger causality p-values and the Pearson correlation coefficients ( $r$ ). As shown in figure 1 (a), Granger causality analysis reveals that all 19 input signals exhibit statistically significant Granger causal relationships with the output signals, with p-values below 0.05. Figure 1 (b) shows that the Pearson correlation coefficients between the input and output signals are also statistically significant, indicating strong linear associations.

For the Granger causality analysis, non-stationarity is common in our signals. Therefore, we tested lags from 1 to 4 and employed four different statistical methods: the SSR-based F test, the SSR-based  $\chi^2$  test, the likelihood ratio (LR) test, and the parameter F test. This resulted in  $4 \times 4$  p-values, from which we selected the minimum value as the final p-value. For the Pearson correlation coefficient, we also introduced a lag term and focused solely on the absolute magnitude of the correlation, disregarding the sign (positive or negative). We tested lags from 0 to 4, and selected the maximum absolute value as the final correlation coefficient  $r$ . The final correlation coefficient  $r_{\text{final}}$  was defined as:

$$r_{\text{final}} = \max_{l \in \{0, 1, 2, 3, 4\}} |r(\{x_l, x_{l+1}, \dots, x_n\}, \{y_0, y_1, \dots, y_{n-l}\})|,$$

where  $r$  denotes the standard Pearson correlation coefficient, and  $l$  is the lag.

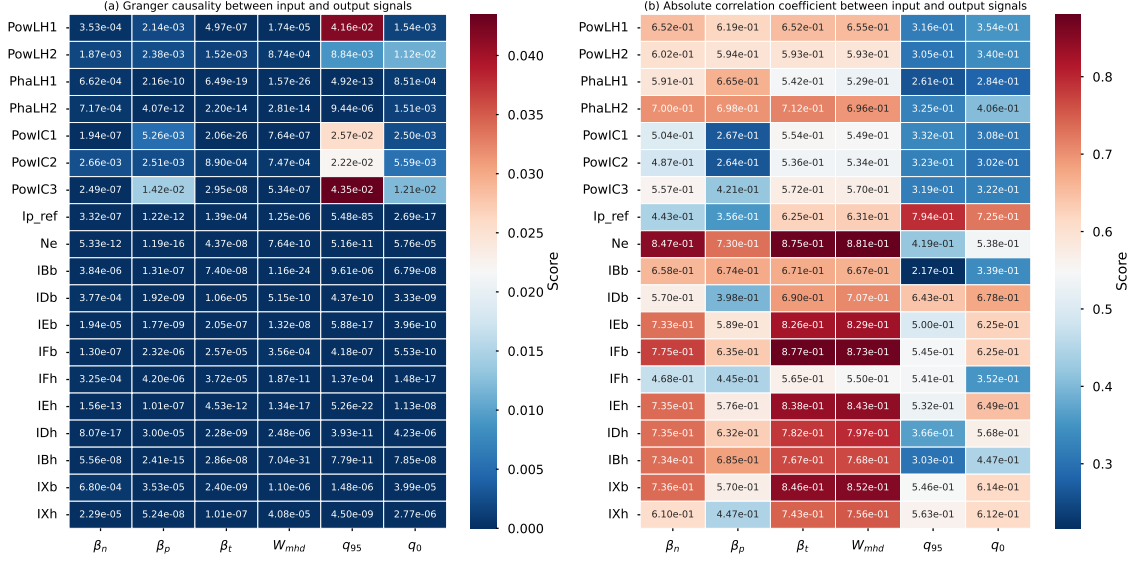


**Figure 1:** The Granger causality and Pearson correlation coefficient between input and output signals. For Granger causality, a smaller coefficient indicates a stronger causal relationship, whereas for the Pearson correlation coefficient, a larger value reflects a stronger linear correlation. PowerLH\* and PhaLH\* are the actual powers and corresponding phases of the LHW system, PowerIC\* is the powers of the ICRH system, Ip is the reference of plasma current, the remaining signals correspond to various locations of the PF coils.

While these statistical tests offer valuable preliminary insights, it is important to note that machine learning models possess strong nonlinear mapping capabilities. Traditional statistical measures such as Granger causality and Pearson correlation capture only specific types of relationships and may not fully reveal the complex dependencies within the data. Therefore, the statistical analysis primarily serves to provide prior knowledge and validate the relevance of the input features. Machine learning methods remain essential for constructing the complex mappings between input and output signals.

### 3. Methods

The machine learning model and its data processing workflow are shown in figure 2. Prior to model input, the raw data are smoothed using a Simple Moving Average (SMA) filter to suppress noise. The SMA operation is defined in equation 1. To accommodate discharge sequences of varying lengths, the data are segmented using a fixed-size sliding window with a window length of 1024 and a step size of 512. This configuration yields a data augmentation ratio of 2, resulting in a total of  $12059 \times 2$  sliced windows, where 2 denotes the augmentation factor introduced by overlapping segmentation. Because the output sequences overlap as shown by the dark blue regions in figure 2, the overlapping segments are averaged to improve numerical stability and prediction accuracy (see Appendix B, figure 6 for supporting evidence). The 550 discharges were randomly divided into training (60%), validation (20%), and test (20%) sets. A strictly chronological split

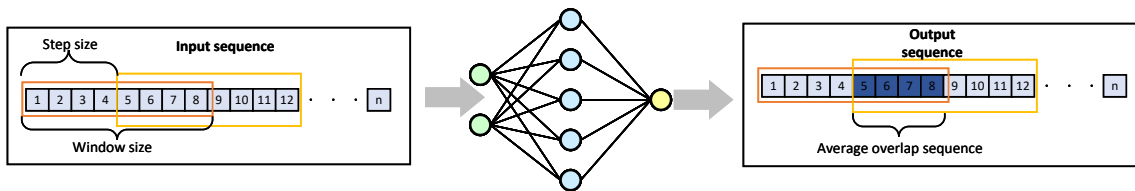


**Figure 2:** The workflow of machine learning model in the present work

**Table 2:** List of tested models with mean squared error (MSE) loss on validation set. All models employ Bayesian optimization to identify relatively optimal architectures. The losses reported in the table correspond to those obtained under each model’s optimal configuration.

Model type	Mean Squared Error (MSE) loss
Multilayer perceptron (MLP)	0.0224
Long Short-Term Memory (LSTM)	0.015
Transformer Encoder	0.011
Transformer Decoder	0.011
<b>Our transformer-based model</b>	<b>0.0096</b>

was not used, as the objective of the present study is to evaluate inter-discharge generalization within the operational envelope represented in the WEST dataset, and to provide a fast surrogate for scenario evaluation and discharge design under conditions similar to those already explored. The SMA filter is defined as:

$$\text{SMA}_t = \frac{1}{w} \sum_{i=-\lfloor w/2 \rfloor}^{\lfloor w/2 \rfloor} x_{t+i}, \quad t = \lfloor w/2 \rfloor + 1, \dots, N - \lfloor w/2 \rfloor \quad (1)$$

where  $x_t$  denotes the input time-series signal of length  $N$ , and  $w$  is the window size of the simple moving average (SMA) filter. This centered formulation ensures that the smoothing operation does not introduce temporal lag or phase shift. The valid index range for  $t$  guarantees that the averaging window lies entirely within the signal boundaries, thereby avoiding boundary artifacts. No padding or extrapolation is applied at the signal edges.

To evaluate the predictive performance of our proposed approach, we established a benchmark suite comprising several machine learning architectures, as shown in table 2. Specifically, we developed and implemented: (i) a classic multilayer perceptron (MLP); (ii) a long short-term memory (LSTM) network, representative of widely used time-series models; (iii) a Transformer encoder based model, which forms the basis for Google’s BERT [49]; (iv) a Transformer decoder based model, as used in OpenAI’s ChatGPT [50, 51]; and (v) a Transformer-based model [52].

All models employed Bayesian optimization [53] to determine relatively optimal architectural configurations. Each model was trained and evaluated using the same 550 discharges. The loss values reported in table 2 correspond to those obtained under each model’s optimal setup. As shown in table 2, our Transformer-based model achieves the lowest mean squared error (MSE) loss among all tested models. In machine learning evaluation, a smaller MSE loss indicates better predictive performance. From a machine learning perspective, this result is consistent with the ability of Transformer models to capture long-range temporal dependencies and complex cross-channel interactions through self-attention mechanisms, which are particularly well suited to the

**Table 3:** Our model hyperparameters

Hyperparameter	Explanation	Best value
$\eta_t$	Learning rate	$1 \times 10^{-3}$
num_heads	Number of heads	8
num_layers	Number of layers	2
Optimizer	Optimizer type	Stochastic Gradient Descent (SGD)
$\eta_{\text{dropout}}$	Dropout rate	0.1
B	Batch size	16
W	Window size	1024
S	Step size	512
Filter	Filter type	Simple moving average
$W_{\text{filter}}$	Window size of the filter	11

multi-signal, long-duration discharge sequences considered in this study. Based on both the superior performance shown in table 2 and these architectural advantages, the Transformer-based model was selected for this work.

Our machine learning model was developed using PyTorch on Red Hat Enterprise Linux 8, running on four A100 GPUs. During model training, we utilized Bayesian algorithm [53] to perform the architectural hyperparameter search. Additionally, we experimented with various optimizers and regularization techniques, ultimately identifying the optimal set of hyperparameters, as shown in table 3. Inference time was further tested on both a consumer-grade RTX 3090 GPU and an A100 GPU, with both achieving similar inference times of  $\sim 0.1$  seconds.

#### 4. Results

This section presents the results and analysis. The results include different types of discharges and the statistical evaluation of six output signals. In this study, we randomly partition the entire dataset into training, validation, and test sets with a ratio of 6:2:2. The machine learning model is trained on the training set, and the optimal model is selected based on its performance on the validation set. The results presented in this section correspond to the model’s performance on the test set, which includes 110 discharges. The final average mean squared error (MSE) on the test set is 0.026, and the coefficient of determination  $R^2$  is 0.94.

Figure 3 shows the model predictions for three typical WEST discharges #57948, #58387, #59490. The duration of these discharges ranges from approximately 10 to 70 seconds, and they involve 2 types of auxiliary heating. Under these conditions, our model can successfully reproduce the entire discharge pulse from the ramp-up, through the flat-top, to the ramp-down phases. However, there is a slight discrepancy in the predictions of  $q_0$  and  $q_{95}$ . We also observe the same phenomenon in statistical plots as shown in figure 4. These quantities exhibit lower accuracy because our input signals do not properly contain the pressure profiles and kinetic measurements. Our goal is to reproduce the tokamak response using signals that can be specified before discharge, these measurements should not be included in the input signals. If  $q_0$  and  $q_{95}$  are not properly constrained, they may be unreliable due to large variances, as the model struggles to reconstruct these parameters. In addition, even under well-controlled experimental conditions with stable wall behavior, identical or highly similar input configurations can still lead to different plasma responses.

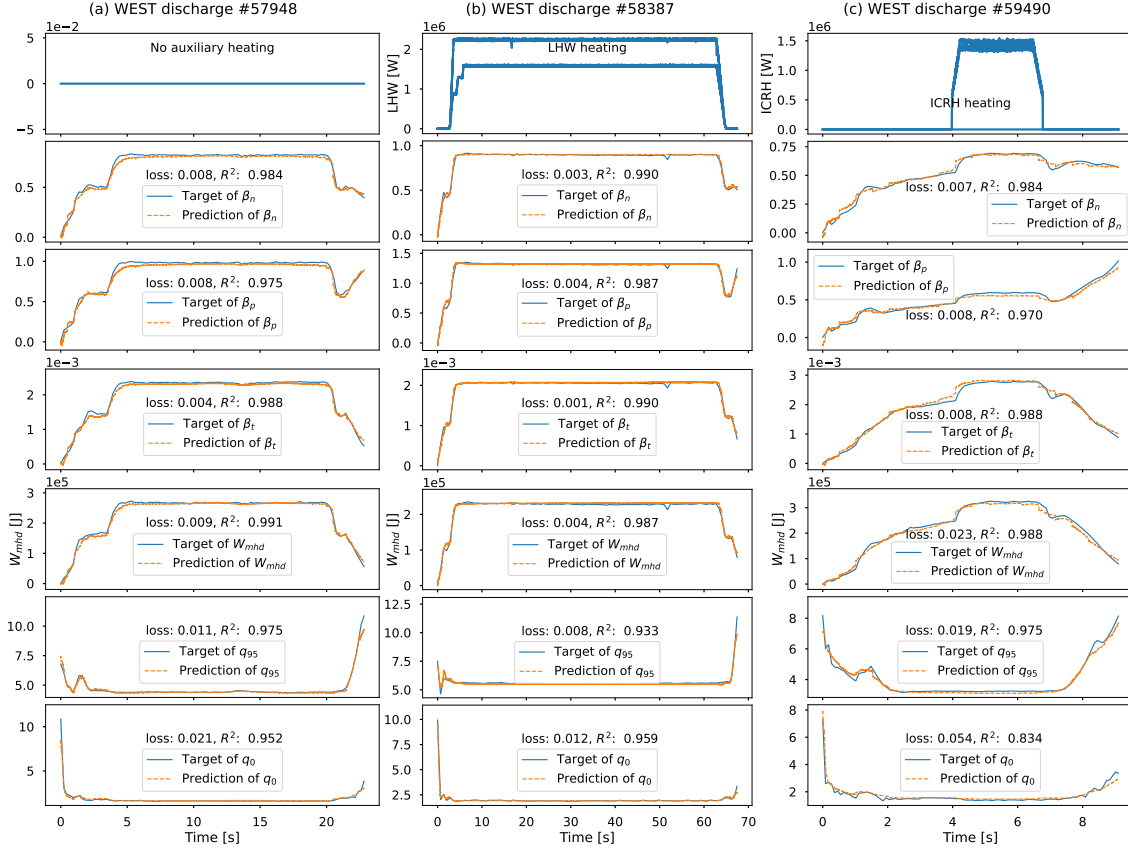


**Figure 3:** Three types of typical discharge prediction in the test set. (a) The Ohmic heating-only discharge. (b) The discharge with LHW heating. (c) The discharge with ICRH heating. The targets represent experimental measurements, while the predictions correspond to the model estimations.

This challenge is particularly pronounced for  $q_0$  and  $q_{95}$ , which depend on the radial distribution of the plasma current density  $j(r)$  [54]. Since most of the input signals do not uniquely determine the internal current redistribution during the discharge, these quantities are weakly identifiable from pre-discharge inputs alone.

As shown in figure 4, we quantitatively evaluate the model performance on the entire test set, which consists of 110 discharges. For each discharge, the target and predicted values are averaged over its duration. Overall, the model demonstrates strong performance across most output parameters, except for  $q_0$  and  $q_{95}$ , where prediction accuracy is relatively lower. A small number of discharges show poor predictive performance. Detailed analysis reveals that these cases are mainly associated with fluctuations in magnetic field coil currents, events that are uncommon and not part of standard tokamak operational planning (e.g., discharge #57821, see Appendix A, figure 7). Such cases deviate from our objective of reproducing plasma responses in conventional discharges and providing reliable references for tokamak scenario design, as these fluctuations are

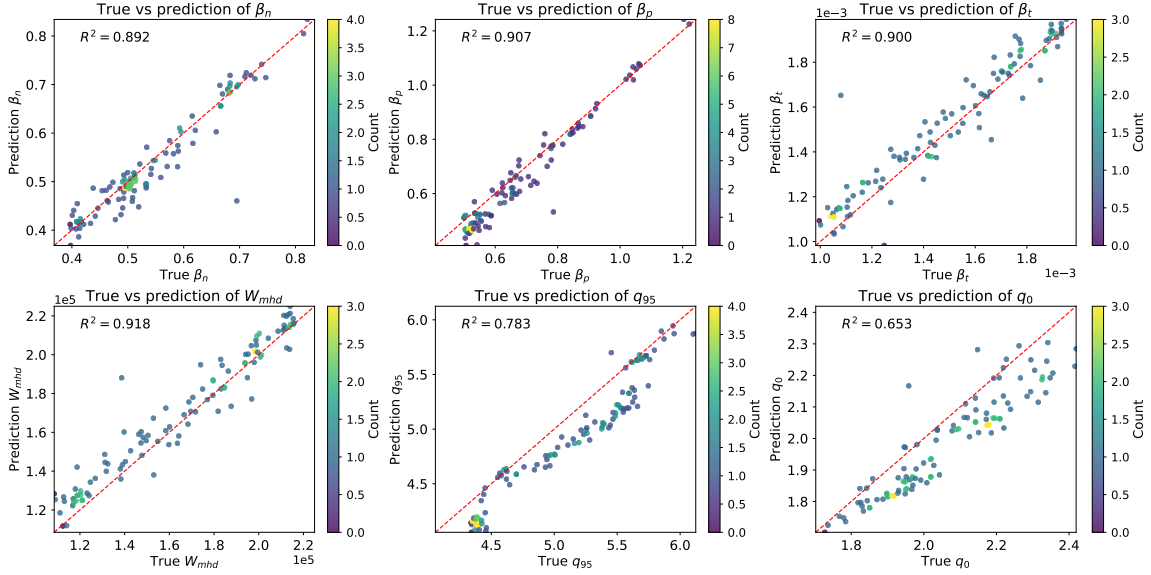


**Figure 4:** Regression plots of the output signals. Both the target and predicted values are averaged over the duration of each discharge. Except for  $q_0$  and  $q_{95}$ , the model achieves a coefficient of determination  $R^2$  greater than 0.890. The performance for  $q_0$  and  $q_{95}$  is lower compared to the other signals.

typically unintended and fall outside the scope of standard design procedures. The systematic underestimation of  $q_0$  and  $q_{95}$  does not originate from a structural limitation of the machine learning model. Similar behavior is observed across different architectures (e.g., in our LSTM-based model tests), indicating that the effect is primarily data-driven. Preprocessing steps such as signal smoothing and overlap-averaging can attenuate rapid temporal variations, leading to reduced peak values near transient phases. In addition, equilibrium reconstruction of  $q$  profiles may introduce asymmetric noise or offsets, which, under an MSE-based training objective, can result in regression-to-the-mean behavior. Together, these factors contribute to the observed underestimation.

In addition, some discharges correspond to rare operational scenarios, such as discharge #60147 (see Appendix A, figure 8), which involves the use of two valid auxiliary heating methods and they are very rare in our dataset. This discharge occurs only three times out of 550 discharges. All of these cases are in the test set. The model’s generalization ability for such unusual and rare discharges remains limited. Handling rare cases is an inherent challenge for machine learning methods. To improve performance in future work, we plan to include more discharges from this scenario to enhance the model’s exposure and learning. We will also explore some data augmentation for the rare and fluctuating discharges, or use some physics-informed method to enhance the ML model’s generalization ability.

## 5. Conclusion and discussion

In this study, we proposed a transformer-based machine learning model for forecasting the behavior of tokamak plasmas based on discharge configurations. The model takes as input the auxiliary

heating power, magnetic field coil currents, plasma current, and line-averaged plasma density. These signals are typically designed or programmed prior to the actual discharge, enabling the model to predict the plasma’s response to the intended operational settings.

The objective of the present work is complementary rather than competitive with real-time physics-based simulation frameworks. By learning the direct mapping between pre-discharge inputs and global plasma responses from a large experimental dataset, the proposed model bypasses explicit transport assumptions and empirical coefficient tuning. This enables fast, fully pre-discharge prediction that reflects the actual behavior of the machine. In this sense, physics-based reduced models answer the question of what should happen according to simplified physical assumptions, whereas the proposed data-driven approach captures what actually happens, as evidenced by historical experimental operation.

The current model focuses on predicting six key global plasma parameters: normalized beta ( $\beta_n$ ), toroidal beta ( $\beta_t$ ), poloidal beta ( $\beta_p$ ), plasma stored energy ( $W_{\text{mhd}}$ ), safety factor at the magnetic axis ( $q_0$ ), and safety factor at the 95% flux surface ( $q_{95}$ ). These quantities serve as essential indicators of plasma performance, stability, and confinement quality. The model demonstrates promising predictive performance and offers potential applications in discharge planning and fast scenario evaluation for tokamak experiments.

The present work can be extended to predict additional plasma parameters, such as the loop voltage ( $V_{\text{loop}}$ ) and internal inductance ( $l_i$ ) or 1D profiles such as density and temperature, which are also important for characterizing plasma behavior and optimizing control strategies. However, a significant challenge lies in obtaining sufficient and diverse data to properly constrain the model and ensure its generalization to a broader range of operational scenarios.

Moreover, purely data-driven models exhibit strong sensitivity to the specific conditions of the device. Consequently, directly applying the model after major hardware modifications or transferring it to a different tokamak remains an unresolved challenge. To address these limitations, future research can explore hybrid approaches that integrate physical knowledge or constraints into the model architecture or training process. Incorporating physics-informed methods has the potential to enhance the model’s robustness and generalization capabilities, particularly for extrapolating to unfamiliar operational regimes.

Additionally, collecting datasets from multiple devices and adopting dimensionless representations for both input and output signals can further improve the cross-device applicability and generalization capability of the model. These approaches align with the broader goal of developing reliable, data-driven surrogate models that can support discharge design, scenario optimization, and real-time plasma control across present and future tokamak devices.

### Data availability statement

The data supporting the findings of this study are owned by WEST/CEA, and the code is jointly owned by WEST/CEA and NTU. Both are available from the corresponding author upon reasonable request.

### Acknowledgments

The computational work for this article was partially performed on resources of the National Supercomputing Centre, Singapore (<https://www.nsc.sg>).

This research is supported by the National Research Foundation, Singapore, the National Natural Science Foundation of China under Grant No. 12505267, the China Postdoctoral Science Foundation under Grant Nos. 2023M743541 and 2023M733545, the Anhui Postdoctoral Scientific Research Program Foundation under Grant No. 2024C997, the Science Foundation of Institute of Plasma Physics, Chinese Academy of Sciences No. DSJJ-2025-11, and WEST team (<http://west.cea.fr/WESTteam>) under the NTU/CEA SAFE (Singapore Alliance with France for Fusion Energy) collaboration agreement.

## **Appendix A. The parameter distributions in our**

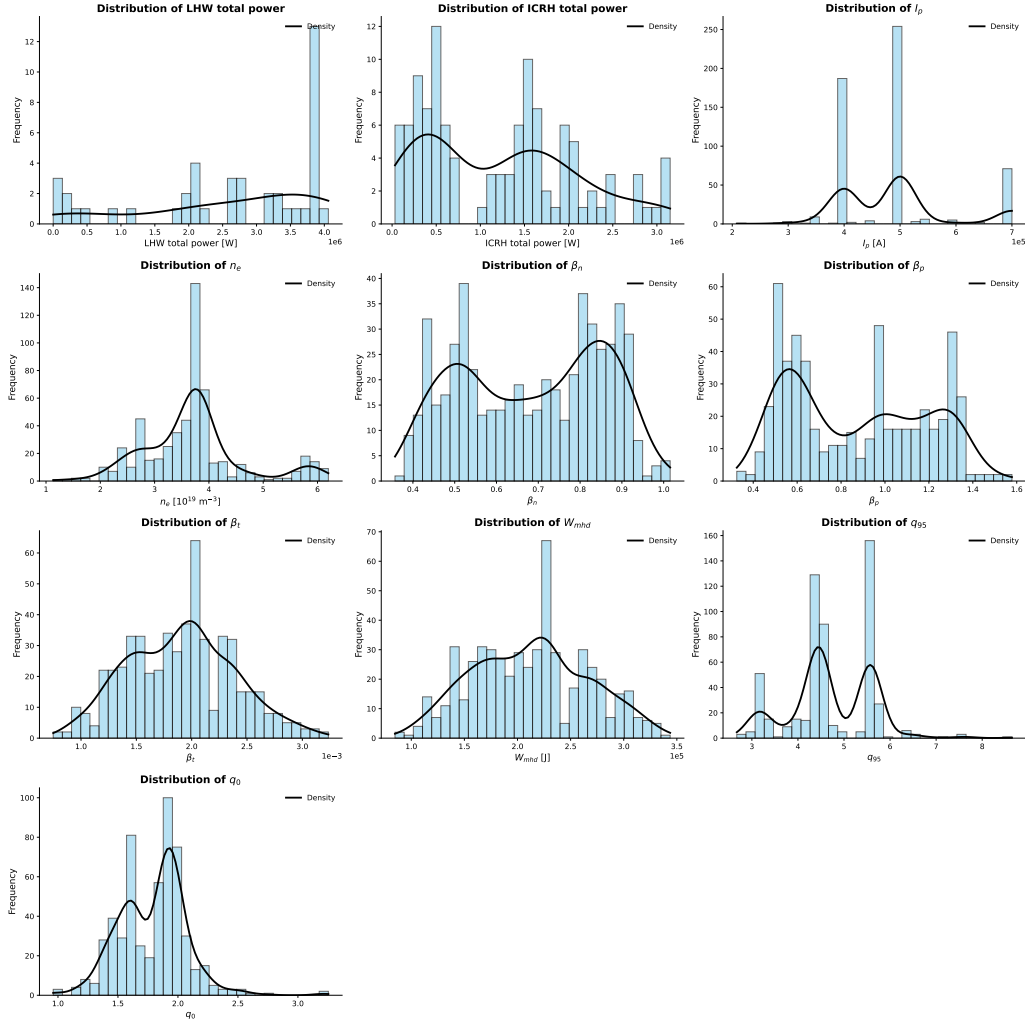


**Figure 5:** Discharge parameter distributions in the whole dataset. All ICRH and LHW discharge with a total power of zero are removed.

## Appendix B. Robustness of reconstruction with respect to sliding-window step size

The final goal of the variance comparison is to understand the trend of variance vs step size. To reduce computing complexity, the variances in the figure are calculated as follows:

To characterize the trend of prediction stability with respect to the sliding-window step size, we define an error-based variance metric as

$$\text{Var}(s) = \frac{1}{LK} \sum_{t=0}^L \sum_{k=1}^K \left( \hat{Y}_{t,k}(s) - Y_{t,k} \right)^2,$$

where  $\hat{Y}_{t,k}(s)$  denotes the predicted value of the  $k$ -th output feature at time step  $t$  obtained

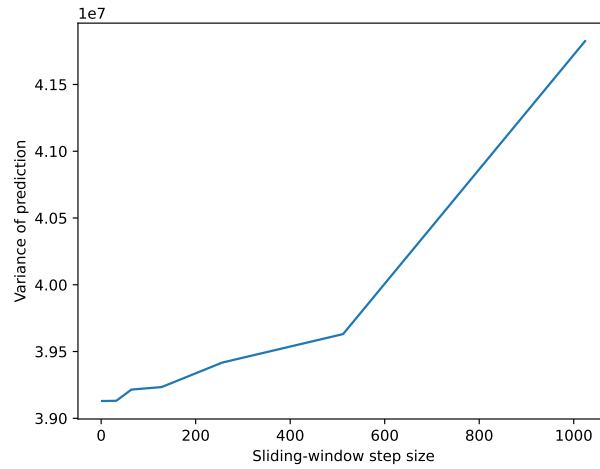


**Figure 6:** Variance of reconstructed predictions as a function of sliding-window step size, evaluated using the same transformer-based model as in the present work.

with step size  $s$ , and  $Y_{t,k}$  is the corresponding ground-truth value.  $L$  is the total number of time samples aggregated over the evaluated discharge segments, and  $K$  is the number of output features, which is  $K = 6$  in this study.

As shown in figure 6, as the step size increases, corresponding to reduced overlap between adjacent windows, the variance of prediction increases, and vice versa. This occurs because partially independent fluctuations across windows are suppressed. This trend indicates that overlap-averaging enhances numerical stability and robustness of the reconstruction.

### Appendix C. The typical bad case of our model.

All signal names of figures 7 and 8 follow the same notation as in figure 1

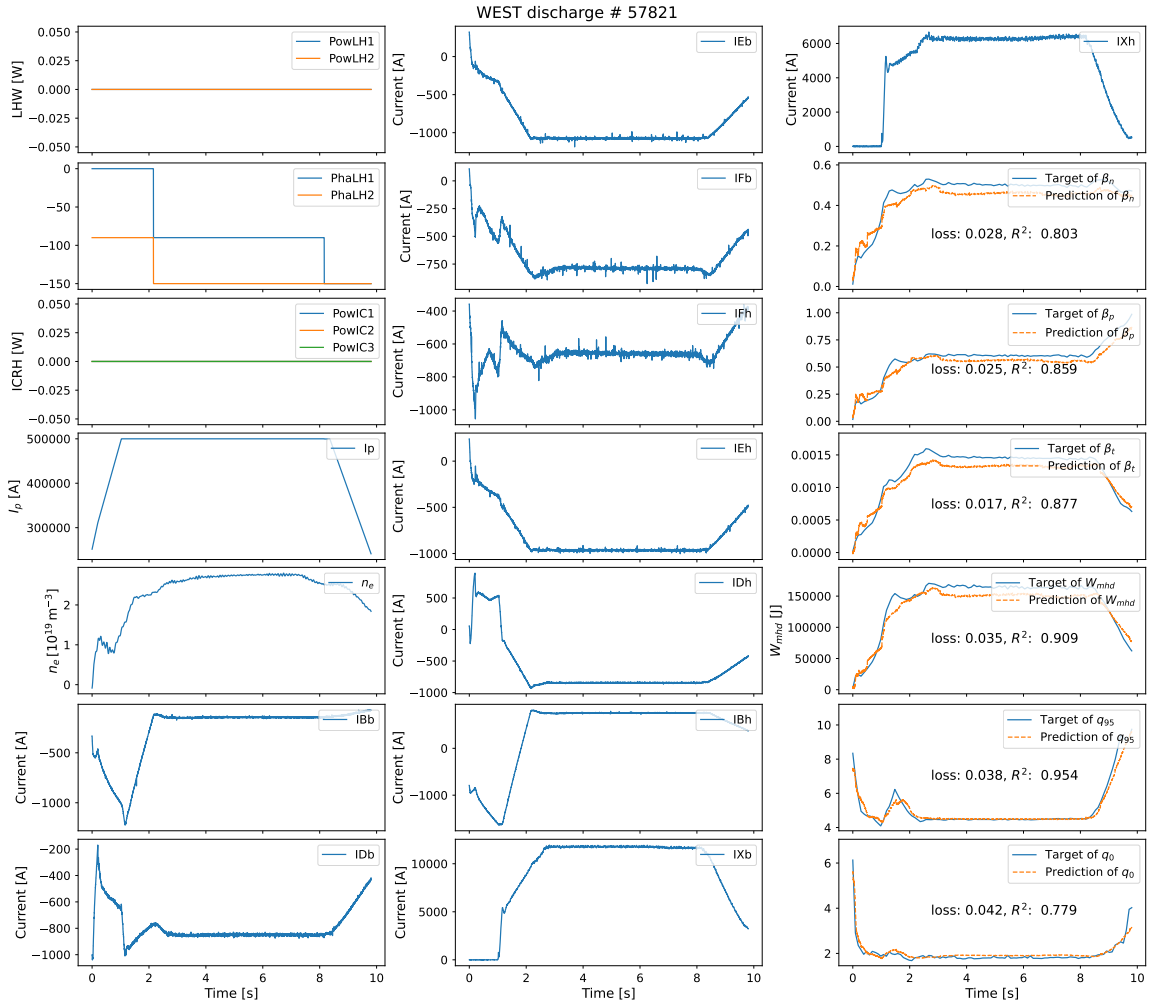


**Figure 7:** WEST discharge #57821. During the time interval 2–6 s, the PF coil currents exhibit a significant spike. This irregularity in the input signals leads to discrepancies in the model’s output predictions.

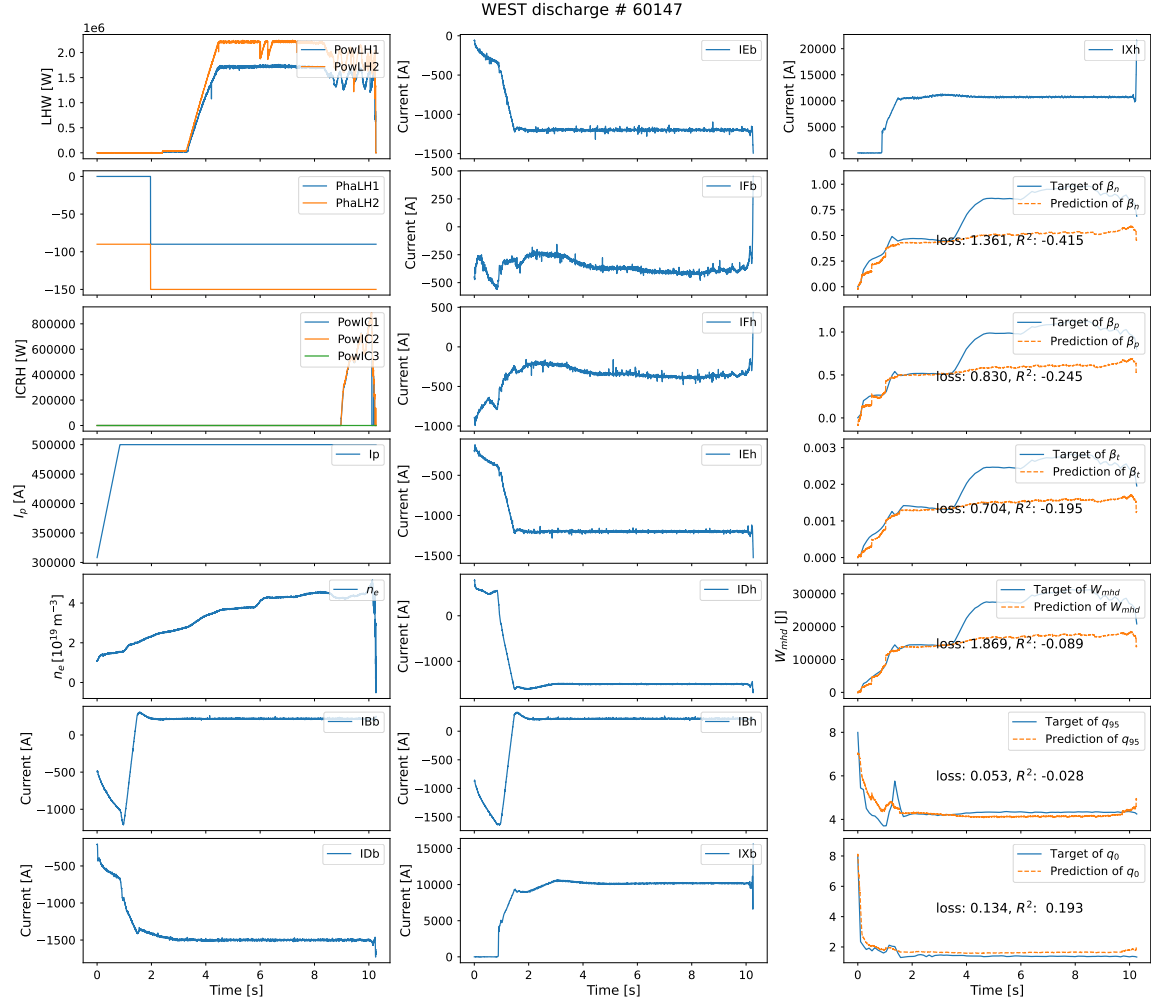


**Figure 8:** WEST discharge #60147. This type of discharge uses two valid auxiliary heating methods, which is very rare in our dataset. Only three out of 550 discharges exhibit such cases, all of which are in the test set. As a result, the model has not learned sufficient information to accurately predict these uncommon discharge scenarios.

## References

- [1] G.L. Falchetto et al. “The European Integrated Tokamak Modelling (ITM) Effort: Achievements and First Physics Results”. In: *Nuclear Fusion* 54.4 (Apr. 2014), p. 043018. ISSN: 0029-5515. DOI: [10.1088/0029-5515/54/4/043018](https://doi.org/10.1088/0029-5515/54/4/043018).
- [2] R V Budny et al. “Predictions of {H}-Mode Performance in {ITER}”. In: *Nuclear Fusion* 48.7 (2008), p. 75005. ISSN: 00295515. DOI: [10.1088/0029-5515/48/7/075005](https://doi.org/10.1088/0029-5515/48/7/075005).

- [3] C E Kessel et al. “Long Pulse High Performance Plasma Scenario Development for the {National} {Spherical} {Torus} {Experiment}”. In: *Physics of Plasmas* 13.5 (2006). ISSN: 1070664X. DOI: [10.1063/1.2177645](https://doi.org/10.1063/1.2177645).
- [4] Blaise Faugeras. “An Overview of the Numerical Methods for Tokamak Plasma Equilibrium Computation Implemented in the NICE Code”. In: *Fusion Engineering and Design* 160 (Nov. 2020), p. 112020. ISSN: 09203796. DOI: [10.1016/j.fusengdes.2020.112020](https://doi.org/10.1016/j.fusengdes.2020.112020).
- [5] J.F. Artaud et al. “The CRONOS Suite of Codes for Integrated Tokamak Modelling”. In: *Nuclear Fusion* 50.4 (Apr. 2010), p. 043001. ISSN: 0029-5515. DOI: [10.1088/0029-5515/50/4/043001](https://doi.org/10.1088/0029-5515/50/4/043001).
- [6] Michele ROMANELLI et al. “JINTRAC: A System of Codes for Integrated Simulation of Tokamak Scenarios”. In: *Plasma and Fusion Research* 9.SPECIALISSUE.2 (2014), pp. 3403023–3403023. ISSN: 1880-6821. DOI: [10.1585/pfr.9.3403023](https://doi.org/10.1585/pfr.9.3403023).
- [7] J F Artaud et al. “Metis: A Fast Integrated Tokamak Modelling Tool for Scenario Design”. In: *Nuclear Fusion* 58.10 (Aug. 2018), p. 105001. ISSN: 17414326. DOI: [10.1088/1741-4326/aad5b1](https://doi.org/10.1088/1741-4326/aad5b1).
- [8] G V Pereverzew et al. “ASTRA. An Automatic System for Transport Analysis in a Tokamak.” In: *IPP-Report IPP 5/98* (1991), p. 147.
- [9] F. Felici et al. “Real-Time Physics-Model-Based Simulation of the Current Density Profile in Tokamak Plasmas”. In: *Nuclear Fusion* 51.8 (Aug. 2011), p. 083052. ISSN: 0029-5515, 1741-4326. DOI: [10.1088/0029-5515/51/8/083052](https://doi.org/10.1088/0029-5515/51/8/083052).
- [10] N Hayashi and JET Team. “Advanced Tokamak Research with Integrated Modeling in {JT}-60 {Upgrade}”. In: *Physics of Plasmas* 17.5 (2010). ISSN: 1070664X. DOI: [10.1063/1.3327917](https://doi.org/10.1063/1.3327917).
- [11] S. Van Mulders et al. “Model-Based Estimation of Tokamak Plasma Profiles and Physics Parameters: Integration with Improved Equilibrium Reconstruction and Experimental Data”. In: *Nuclear Fusion* 66.2 (Feb. 2026), p. 026026. ISSN: 0029-5515, 1741-4326. DOI: [10.1088/1741-4326/ae2c0a](https://doi.org/10.1088/1741-4326/ae2c0a).
- [12] Cristina Rea et al. “Exploratory Machine Learning Studies for Disruption Prediction Using Large Databases on DIII-D”. In: *Fusion Science and Technology* 74.1-2 (2018), pp. 89–100. ISSN: 19437641. DOI: [10.1080/15361055.2017.1407206](https://doi.org/10.1080/15361055.2017.1407206).
- [13] Julian Kates-Harbeck et al. “Predicting Disruptive Instabilities in Controlled Fusion Plasmas through Deep Learning”. In: *Nature* 568.7753 (Apr. 2019), pp. 526–531. ISSN: 0028-0836. DOI: [10.1038/s41586-019-1116-4](https://doi.org/10.1038/s41586-019-1116-4).
- [14] Wei Zheng et al. “Disruption Prediction for Future Tokamaks Using Parameter-Based Transfer Learning”. In: *Communications Physics* 6.1 (July 2023), p. 181. ISSN: 2399-3650. DOI: [10.1038/s42005-023-01296-9](https://doi.org/10.1038/s42005-023-01296-9).
- [15] W. Zheng et al. “Hybrid Neural Network for Density Limit Disruption Prediction and Avoidance on J-TEXT Tokamak”. In: *Nuclear Fusion* 58.5 (Mar. 2018), p. 56016. DOI: [10.1088/1741-4326/aaad17](https://doi.org/10.1088/1741-4326/aaad17).
- [16] Chengshuo Shen et al. “Cross-Tokamak Disruption Prediction Based on Domain Adaptation”. In: *Nuclear Fusion* 64.6 (June 2024), p. 066036. ISSN: 0029-5515, 1741-4326. DOI: [10.1088/1741-4326/ad3e12](https://doi.org/10.1088/1741-4326/ad3e12).
- [17] C. Shen et al. “IDP-PGFE: An Interpretable Disruption Predictor Based on Physics-Guided Feature Extraction”. In: *Nuclear Fusion* 63.4 (Apr. 2023), p. 046024. ISSN: 0029-5515. DOI: [10.1088/1741-4326/acbe0f](https://doi.org/10.1088/1741-4326/acbe0f).

- [18] Jonas Degraeve et al. “Magnetic Control of Tokamak Plasmas through Deep Reinforcement Learning”. In: *Nature* 602.7897 (Feb. 2022), pp. 414–419. ISSN: 0028-0836. DOI: [10.1038/s41586-021-04301-9](https://doi.org/10.1038/s41586-021-04301-9).
- [19] Chenguang Wan et al. “A High-Fidelity Surrogate Model for the Ion Temperature Gradient (ITG) Instability Using a Small Expensive Simulation Dataset”. In: *Nuclear Fusion* 65.5 (Apr. 2025), p. 054001. ISSN: 0029-5515, 1741-4326. DOI: [10.1088/1741-4326/adc7c9](https://doi.org/10.1088/1741-4326/adc7c9).
- [20] K. L. van de Plassche et al. “Fast Modeling of Turbulent Transport in Fusion Plasmas Using Neural Networks”. In: *Physics of Plasmas* 27.2 (Feb. 2020), p. 022310. ISSN: 1070-664X. DOI: [10.1063/1.5134126](https://doi.org/10.1063/1.5134126).
- [21] Jaemin Seo et al. “Avoiding Fusion Plasma Tearing Instability with Deep Reinforcement Learning”. In: *Nature* 626.8000 (Feb. 2024), pp. 746–751. ISSN: 0028-0836. DOI: [10.1038/s41586-024-07024-9](https://doi.org/10.1038/s41586-024-07024-9).
- [22] Chenguang Wan et al. “A Machine-Learning-Based Tool for Last Closed-Flux Surface Reconstruction on Tokamaks”. In: *Nuclear Fusion* 63.5 (May 2023), p. 056019. ISSN: 0029-5515. DOI: [10.1088/1741-4326/acbfcc](https://doi.org/10.1088/1741-4326/acbfcc).
- [23] Chenguang Wan et al. “Predict the Last Closed-Flux Surface Evolution without Physical Simulation”. In: *Nuclear Fusion* 64.2 (Jan. 2024), p. 026014. ISSN: 0029-5515. DOI: [10.1088/1741-4326/ad171f](https://doi.org/10.1088/1741-4326/ad171f).
- [24] D. J. Clayton et al. “Electron Temperature Profile Reconstructions from Multi-Energy SXR Measurements Using Neural Networks”. In: *Plasma Physics and Controlled Fusion* 55.9 (Sept. 2013), p. 095015. ISSN: 0741-3335. DOI: [10.1088/0741-3335/55/9/095015](https://doi.org/10.1088/0741-3335/55/9/095015).
- [25] Semin Joung et al. “Deep Neural Network Grad–Shafranov Solver Constrained with Measured Magnetic Signals”. In: *Nuclear Fusion* 60.1 (Jan. 2020), p. 016034. ISSN: 0029-5515, 1741-4326. DOI: [10.1088/1741-4326/ab555f](https://doi.org/10.1088/1741-4326/ab555f).
- [26] E Coccoresse et al. “Identification of Noncircular Plasma Equilibria Using a Neural Network Approach”. In: *Nuclear Fusion* 34.10 (Oct. 1994), pp. 1349–1363. ISSN: 0029-5515. DOI: [10.1088/0029-5515/34/10/I05](https://doi.org/10.1088/0029-5515/34/10/I05).
- [27] B Ph. van Milligen et al. “Neural Network Differential Equation and Plasma Equilibrium Solver”. In: *Physical Review Letters* 75.20 (Nov. 1995), pp. 3594–3597. ISSN: 0031-9007. DOI: [10.1103/PhysRevLett.75.3594](https://doi.org/10.1103/PhysRevLett.75.3594).
- [28] Minglong Wang et al. “Time Series Extrinsic Regression for Reconstructing Missing Electron Temperature in Tokamak”. In: *Nuclear Fusion* 65.7 (May 2025), p. 076008. ISSN: 0029-5515, 1741-4326. DOI: [10.1088/1741-4326/addb5f](https://doi.org/10.1088/1741-4326/addb5f).
- [29] Jia Huang et al. “Development of Real-Time Density Profile Inversion with Deep Neural Network Model for Multi-Bands X-mode Polarization Reflectometer on EAST”. In: *Plasma Physics and Controlled Fusion* 67 (Apr. 2025), p. 055002. ISSN: 0741-3335, 1361-6587. DOI: [10.1088/1361-6587/adc830](https://doi.org/10.1088/1361-6587/adc830).
- [30] O Barana et al. “Neural Networks for Real Time Determination of Radiated Power in JET”. In: *Review of Scientific Instruments* 73.5 (May 2002), pp. 2038–2043. ISSN: 0034-6748. DOI: [10.1063/1.1463714](https://doi.org/10.1063/1.1463714).
- [31] Enliang Gao et al. “Bayesian Neural Networks for Predicting Tokamak Energy Confinement Time with Uncertainty Quantification”. In: *Nuclear Fusion* 65.08 (July 2025), p. 084001. ISSN: 0029-5515, 1741-4326. DOI: [10.1088/1741-4326/ade8fd](https://doi.org/10.1088/1741-4326/ade8fd).

- [32] A Murari et al. “On the Identification of Instabilities with Neural Networks on JET”. In: *Nuclear Instruments and Methods in Physics Research Section A: Accelerators, Spectrometers, Detectors and Associated Equipment* 720 (Aug. 2013), pp. 2–6. ISSN: 01689002. DOI: [10.1016/j.nima.2013.03.039](https://doi.org/10.1016/j.nima.2013.03.039).
- [33] M.D. Boyer et al. “Real-Time Capable Modeling of Neutral Beam Injection on NSTX-U Using Neural Networks”. In: *Nuclear Fusion* 59.5 (May 2019), p. 056008. ISSN: 0029-5515. DOI: [10.1088/1741-4326/ab0762](https://doi.org/10.1088/1741-4326/ab0762).
- [34] F. Matos et al. “Plasma Confinement Mode Classification Using a Sequence-to-Sequence Neural Network with Attention”. In: *Nuclear Fusion* 61.4 (Apr. 2021), p. 046019. ISSN: 0029-5515. DOI: [10.1088/1741-4326/abe370](https://doi.org/10.1088/1741-4326/abe370).
- [35] A. Murari et al. “Machine Learning for the Identification of Scaling Laws and Dynamical Systems Directly from Data in Fusion”. In: *Nuclear Instruments and Methods in Physics Research Section A: Accelerators, Spectrometers, Detectors and Associated Equipment* 623.2 (Nov. 2010), pp. 850–854. ISSN: 01689002. DOI: [10.1016/j.nima.2010.02.080](https://doi.org/10.1016/j.nima.2010.02.080).
- [36] P. Gaudio et al. “An Alternative Approach to the Determination of Scaling Law Expressions for the L-H Transition in Tokamaks Utilizing Classification Tools Instead of Regression”. In: *Plasma Physics and Controlled Fusion* 56.11 (Oct. 2014), p. 114002. DOI: [10.1088/0741-3335/56/11/114002](https://doi.org/10.1088/0741-3335/56/11/114002).
- [37] A.D. Maris et al. “Correlation of the L-mode Density Limit with Edge Collisionality”. In: *Nuclear Fusion* 65.1 (Jan. 2025), p. 016051. ISSN: 0029-5515, 1741-4326. DOI: [10.1088/1741-4326/ad90f0](https://doi.org/10.1088/1741-4326/ad90f0).
- [38] Yue Yu et al. “Deep Learning-Enabled Real-Time Prediction of Impurity-Induced Detachment in EAST”. In: *Plasma Physics and Controlled Fusion* 67.2 (Feb. 2025), p. 025026. ISSN: 0741-3335, 1361-6587. DOI: [10.1088/1361-6587/adab18](https://doi.org/10.1088/1361-6587/adab18).
- [39] Alvin Garcia et al. “Artificial Intelligence-Based Predictive Modeling for Imaging Neutral Particle Analyzers on the DIII-D Tokamak”. In: *Nuclear Fusion* 65.5 (Apr. 2025), p. 056015. ISSN: 0029-5515, 1741-4326. DOI: [10.1088/1741-4326/adc58b](https://doi.org/10.1088/1741-4326/adc58b).
- [40] Yunfei Ling et al. “PaMMA-Net: Plasmas Magnetic Measurement Evolution Based on Data-Driven Incremental Accumulative Prediction”. In: *Nuclear Fusion* 65.10 (Oct. 2025), p. 106027. ISSN: 0029-5515, 1741-4326. DOI: [10.1088/1741-4326/ae0655](https://doi.org/10.1088/1741-4326/ae0655).
- [41] Chenguang Wan et al. “EAST Discharge Prediction without Integrating Simulation Results”. In: *Nuclear Fusion* 62.12 (Dec. 2022), p. 126060. ISSN: 17414326. DOI: [10.1088/1741-4326/ac9c1a](https://doi.org/10.1088/1741-4326/ac9c1a).
- [42] Chenguang Wan et al. “Experiment Data-Driven Modeling of Tokamak Discharge in EAST”. In: *Nuclear Fusion* 61.6 (June 2021), p. 066015. ISSN: 0029-5515. DOI: [10.1088/1741-4326/abf419](https://doi.org/10.1088/1741-4326/abf419).
- [43] Ian Char et al. *Full Shot Predictions for the DIII-D Tokamak via Deep Recurrent Networks*. Apr. 2024. DOI: [10.48550/arXiv.2404.12416](https://doi.org/10.48550/arXiv.2404.12416).
- [44] P. Moreau et al. “The New Magnetic Diagnostics in the WEST Tokamak”. In: *Review of Scientific Instruments* 89.10 (Oct. 2018), 10J109. ISSN: 0034-6748, 1089-7623. DOI: [10.1063/1.5036537](https://doi.org/10.1063/1.5036537).
- [45] Christophe Bouchand et al. “The Data Acquisition System of WEST’s New Thomson Scattering Diagnostics”. In: *IEEE Transactions on Nuclear Science* 72.3 (Mar. 2025), pp. 575–583. ISSN: 0018-9499, 1558-1578. DOI: [10.1109/TNS.2024.3470868](https://doi.org/10.1109/TNS.2024.3470868).

- [46] O. Meyer et al. “Visible Spectroscopy Diagnostics for Tungsten Source Assessment in the WEST Tokamak: First Measurements”. In: *Review of Scientific Instruments* 89.10 (Oct. 2018), p. 10D105. ISSN: 0034-6748, 1089-7623. DOI: [10.1063/1.5035566](https://doi.org/10.1063/1.5035566).
- [47] C. Gil et al. “Renewal of the Interfero-Polarimeter Diagnostic for WEST”. In: *Fusion Engineering and Design* 140 (Mar. 2019), pp. 81–91. ISSN: 09203796. DOI: [10.1016/j.fusengdes.2019.02.003](https://doi.org/10.1016/j.fusengdes.2019.02.003).
- [48] Rémy Nouailletas et al. “WEST Plasma Control System Status”. In: *Fusion Engineering and Design* 192 (July 2023), p. 113582. ISSN: 09203796. DOI: [10.1016/j.fusengdes.2023.113582](https://doi.org/10.1016/j.fusengdes.2023.113582).
- [49] Jacob Devlin et al. “BERT: Pre-training of Deep Bidirectional Transformers for Language Understanding”. In: *Mlm* (Oct. 2018). DOI: [10.48550/arXiv.1810.04805](https://doi.org/10.48550/arXiv.1810.04805).
- [50] OpenAI et al. *GPT-4 Technical Report*. Mar. 2024. DOI: [10.48550/arXiv.2303.08774](https://doi.org/10.48550/arXiv.2303.08774).
- [51] Tom Brown et al. “Language Models Are Few-Shot Learners”. In: *Advances in Neural Information Processing Systems*. Ed. by H. Larochelle et al. Vol. 33. Virtual Event: Curran Associates, Inc., 2020, pp. 1877–1901. ISBN: 978-1-7138-2954-6.
- [52] Ashish Vaswani et al. “Attention Is All You Need”. In: *Advances in Neural Information Processing Systems*. Vol. 30. California, USA: Curran Associates, Inc., Dec. 2017. ISBN: 978-1-5108-6096-4.
- [53] James Bergstra et al. “Algorithms for Hyper-Parameter Optimization”. In: *Advances in Neural Information Processing Systems*. Ed. by J Shawe-Taylor et al. Vol. 24. Granada, Spain: Curran Associates, Inc., 2011.
- [54] F. M. Levinton et al. “ $Q$  -Profile Measurements in the Tokamak Fusion Test Reactor\*”. In: *Physics of Fluids B: Plasma Physics* 5.7 (July 1993), pp. 2554–2561. ISSN: 0899-8221. DOI: [10.1063/1.860743](https://doi.org/10.1063/1.860743).